Supporting Information

Covalent Organic Framework-based Nanocomposite for Synergetic Photo-, Chemodynamic- and Immunotherapies

Sainan Liu,[1,2] *Ying Zhou*,[1] *Chunling Hu*,[1,2] *Lihan Cai*,[1,2] and *Maolin Pang*[1,2*]

[1]State Key Laboratory of Rare Earth Resource Utilization, Changchun Institute of Applied Chemistry, Chinese Academy of Science, Changchun 130022, PR China

[2]University of Science and Technology of China, Hefei 230026, PR China

*Corresponding Author: mlpang@ciac.ac.cn

Experimental Section

Chemicals and Materials. 2,5-dimethoxyterephthaldehyde ($C_{10}H_{10}O_4$, AR, Jilin Chinese Academy of Sciences-Yanshen Technology Co. Ltd), 1,3,5-tris(4-aminophenyl)benzene ($C_{24}H_{21}N_3$, AR, 98%, Alpha), Methanol (AR, Beijing Chemical Works), Acetonitrile(CH_3CN, 99.8%, Vetec), Acetic acid (CH_3COOH, AR, Beijng Chemical Works), Ferric chloride ($FeCl_3$, AR, Aladdin), *p*-Phenylenediamine ($C_6H_8N_2$, AR, 97.0%, Aladdin) NH_2-PEG-2000-COOH (Huawei ruike chemical Co., Ltd).

Characterization

Powder X-ray diffraction (PXRD) studies were performed on a Rigaku MiniFlex 600 diffractometer with graphite monochromatized Cu Kα radiation (λ = 0.15405 nm). The sample was scanned at a scanning rate of 8°/min in the 2θ range from 2 to 40° at room temperature. Field emission scanning electron microscope (FE-SEM, S-4800, Hitachi) equipped with an energy dispersive X-ray (EDX) spectrometer was used to characterize the morphology of the sample. Transmission electron microscopy (TEM) images were obtained on a FEI Tecnai G2 S-Twin with a field emission gun operating at 200 kV. Thermogravimetric analysis data was recorded on a TGA 500 thermogravimetric analyzer by heating with a rate of 10 ℃/min under the nitrogen atmosphere (60 mL/min). Fourier transform infrared spectroscopy (FT-IR) was measured on a Vertex PerkinElmer 580 BIR spectrophotometer (Bruker) using the KBr tabletting technique. The sample was securely packaged to obtain a transparent film. The UV-Vis adsorption spectral values were obtained on a U-3310 spectrophotometer (Hitachi). The X-ray photoelectron spectra (XPS) were taken on a VG ESCALAB MK II electron energy spectrometer using Mg KR (1253.6 eV) as the X-ray excitation source. Dynamic light scattering (DLS) experiment was measured by Malvern Zeta Sizer-Nano ZS90 instrument at 25 ℃. MTT experiments were carried out using a microplate reader (Thermo Multiskan MK3).

Photothermal Heating Experiments on CFAP. CFAP aqueous solutions with different concentrations (0-500 μg mL^{-1}) were suspended in different wells of a 96-well plate, and irradiated with an 808 nm laser (1.56 W cm^{-2}) for 5 min. The temperatures were carefully measured every 15 s by a digital thermometer with a thermocouple probe. In order to test the photostability of CFAP, the heating and cooling (ON-OFF) cycle was repeated for more than five times with 808 nm laser

irradiation (1.56 W cm^{-2}). In each heating-cooling cycle, the CFAP aqueous solution was irradiated for 10 min first and then followed by a 15 min cooling period until the temperature reached room temperature again. The in vivo analysis of photothermal effect was achieved by intratumor-injected CFAP (200 μg mL^{-1}) into tumor BALB/C mice. All of the temperatures were recorded by a photothermal camera every 15 s.

Photothermal Conversion Efficiency of CFAP. The photothermal conversion efficiency was determined based on the protocol reported before. First, the CFAP aqueous solution was irradiated by an 808 nm laser for 10 min (1.56 W cm^{-2}) and followed by a natural cooling period. During the cooling process, all of the temperatures were also carefully monitored every 15 s by a thermometer with a thermocouple probe. The photothermal conversion efficiency (η) was calculated by the following equation:

$$\eta = \frac{hS\Delta T_{max} - Q_{Dis}}{I(1 - 10^{-A_{808}})}$$

where h is the heat transfer coefficient, S is the surface area of the container, T_{max} is the equilibrium temperature after 10 min irradiation, Q_{Dis} expresses the heat dissipation by the test cell, I is 808 nm CW laser power (1.2 W/cm^2), and A_{808} is the absorbance of the CFAP aqueous solution at 808 nm. The value of hS is determined according to the following equation:

$$hS = \frac{m_d C_d}{\tau_s}$$

where m_d is the mass (0.4 g) and C_d is the heat capacity (4.2 J/g) of the aqueous solvent, $\boldsymbol{\tau_s}$ is the sample system time constant, and $\boldsymbol{\theta}$ is defined as the ratio of ΔT and ΔT_{max}.

$$\mathbf{t} = -\boldsymbol{\tau_s}(\mathbf{ln}\boldsymbol{\theta})$$

The photothermal efficiency and related data of CFAP was shown in Table S1.

Cellular Internalization of CFAP. In order to study the cellular uptake of CFAP, rhodamine B (RhB)-loaded CFAP was prepared. 20 mg of 1-(3-Dimethylaminopropyl)-3-ethylcarbodiimide hydrochloride (EDC), 6 mg of N-Hydroxysuccinimide (NHS) and 10 mg of rhodamine were dissolved in 5 mL of deionized water, stirred at room temperature for 1 h, and then 10 mL of CFAP solution in deionized water (about 10 mg) was added and stirred overnight. The product was washed with deionized water until the supernatant was nearly colorless.

CT26 cells were incubated with rhodamine B (RhB)-loaded CFAP (50 μg mL^{-1}) for 1, 2, 4 h, respectively. It was then washed with PBS for three times. The nuclei were labeled with 4,6-diamino-2-phenylindole (DAPI) for 10 min and then observed under a fluorescence microscope.

Intracellular ROS Detection. CT26 cells were incubated with CFAP (50 μg mL^{-1}) for 24 h, and irradiated with 650 nm laser (0.72 W cm^{-2}) and 808 nm laser (1.56 W cm^{-2}) for 10 min, respectively. Then the culture medium was replaced and RPMI containing DCFH-DA (10×10^{-6} M) was added and further incubated in the dark for 20 min. Then it was washed by PBS for three times and observed under a fluorescence microscope.

In Vitro Cytotoxicity Assay. In order to study the in vitro biocompatibility of CFAP, L929 cells were seeded into 96-well plates with a density of 6000 cells per well and cultured in RPMI for 24 h. The original medium was then sucked out and the new medium containing different concentrations of CFAP was added again. After the cells were incubated for another 24 h, the medium inside was again discarded and re-added with fresh RPMI containing 10 μL of the standard methyl thiazolyl tetrazolium (MTT). After placing the plates in the dark for 4 h, 150 μL of DMSO was added to each well and the absorption value of the medium was measured by a microplate reader at the wavelength of 490 nm.

To study the in vitro CDT and PDT as well as PTT effect of CFAP, four groups of CT26 cells were seeded into 96-well plates with a density of 6000 cells per well and cultured in RPMI for 24 h. The original medium was then sucked out and the new medium containing different concentrations of CFAP was added again, respectively. After the cells were incubated for 4 h, the medium inside was again discarded and re-added with fresh RPMI. One group of CT26 cells were not irradiated and the other three groups of CT26 cells were irradiated with a 650 nm laser (0.72 W cm^{-2}), an 808 nm laser (1.56 W cm^{-2}) and a combination of 650 nm laser (0.72 W cm^{-2}) and 808 nm laser (1.56 W cm^{-2}) for 5 min, respectively. Then the cells were incubated for another 24 h before the MTT assay was used to detect the cell viability.

Cell Apoptosis of CFAP Nanoparticles. To study the cell apoptosis process of, the Annexin V-FITC/PI Apoptosis Detection Kit was used. CT26 cells were treated with control, 650 nm, 808 nm, 650 nm + 808 nm, CFAP (50 μg mL^{-1}), CFAP + 650 nm (50 μg mL^{-1}, 0.72 W cm^{-1}), CFAP + 808 nm (50 μg mL^{-1}, 1.56 W cm^{-1}) and CFAP + 650 nm + 808 nm (50 μg mL^{-1}, 0.72 W cm^{-1} and 1.56 W cm^{-1}), respectively, and then the

cells were incubated in 6-well plates overnight. After that, the cells were harvested and washed with PBS, and then resuspended with binding buffer (400 μL). At last, 5 μL of Annexin V-FITC and 5 μL of PI were utilized to stain the samples for 15 min and 5 min in the dark, respectively. The cell apoptosis process was monitored via a flow cytometer.

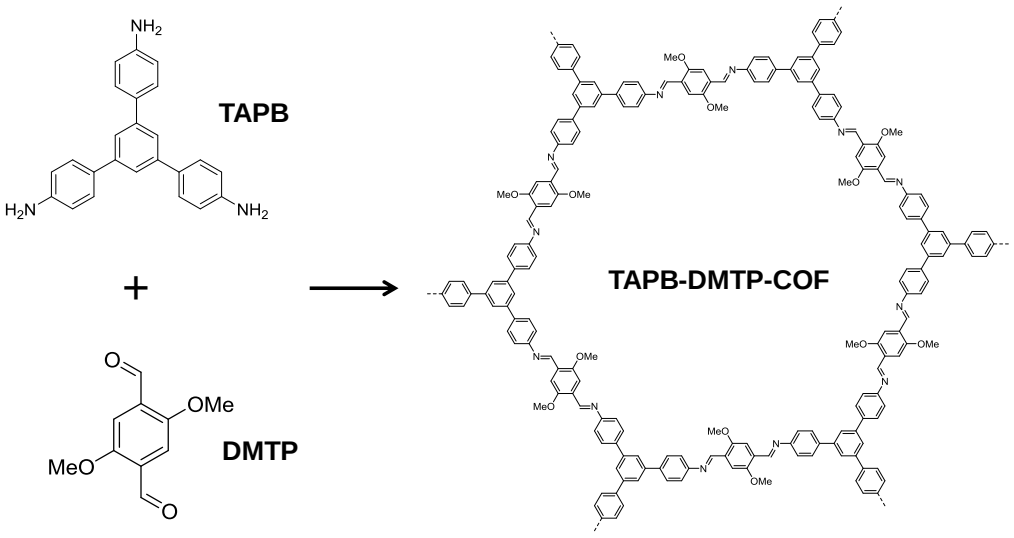

Figure S1. Schematic illustration and molecular structure of the TAPB-DMTP-COF.

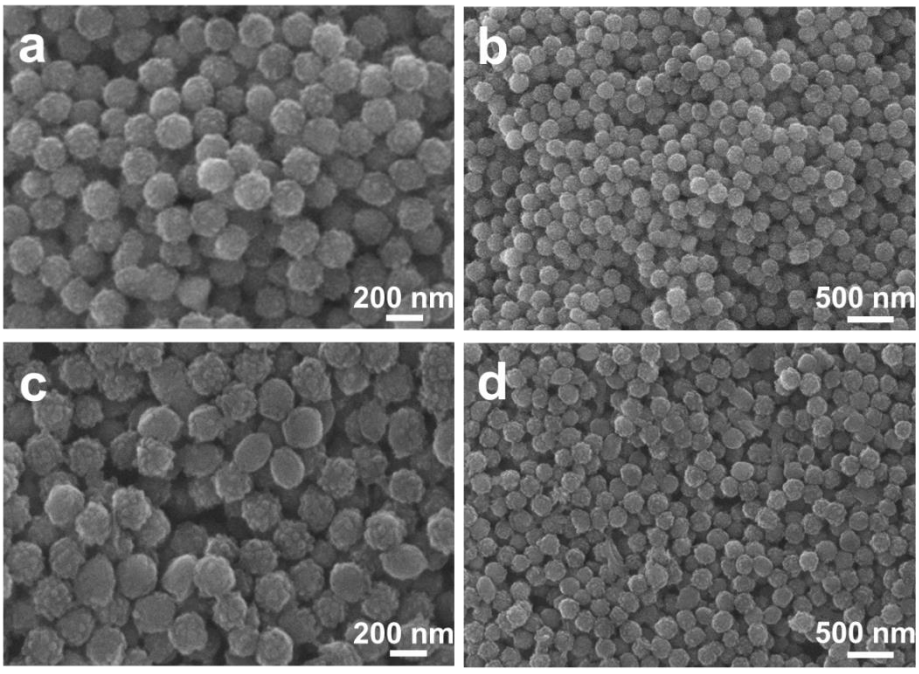

Figure S2. Additional SEM images of COF (a and b) and CFA (c and d).

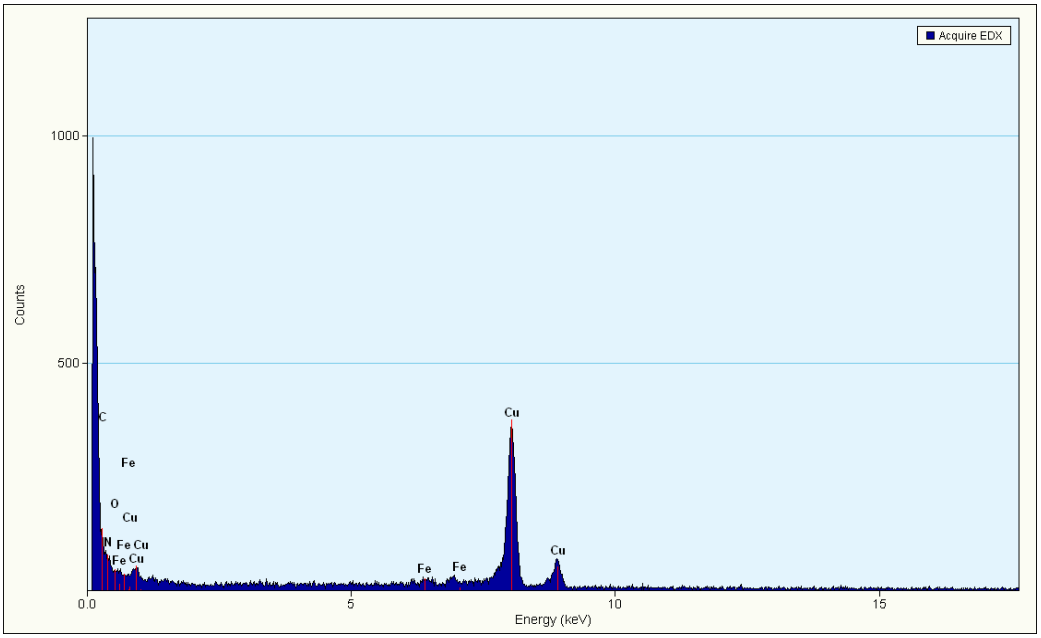

Figure S3. Energy dispersive spectrometer (EDS) of CFA.

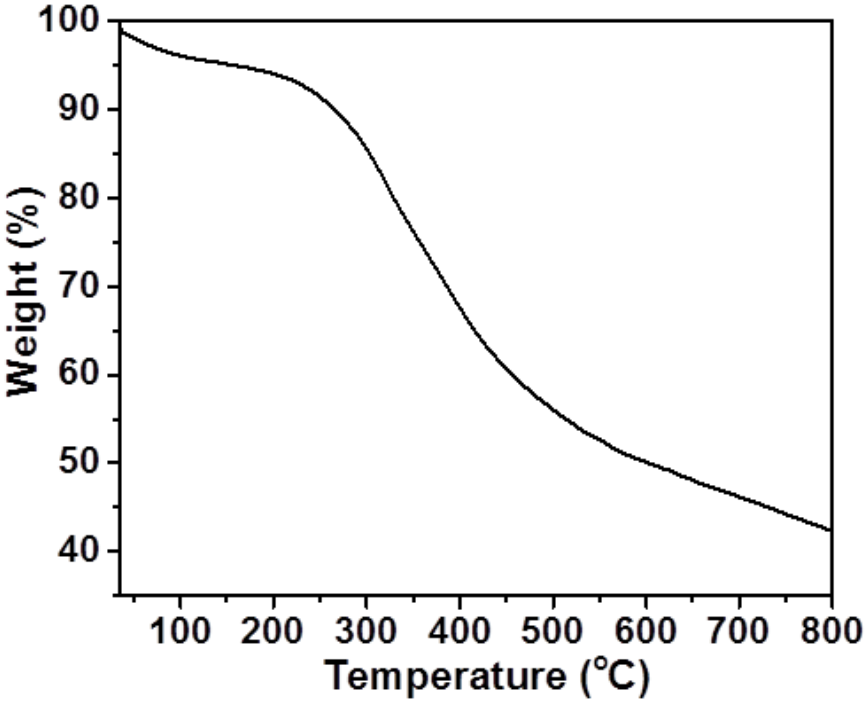

Figure S4. The TGA curve of CFA.

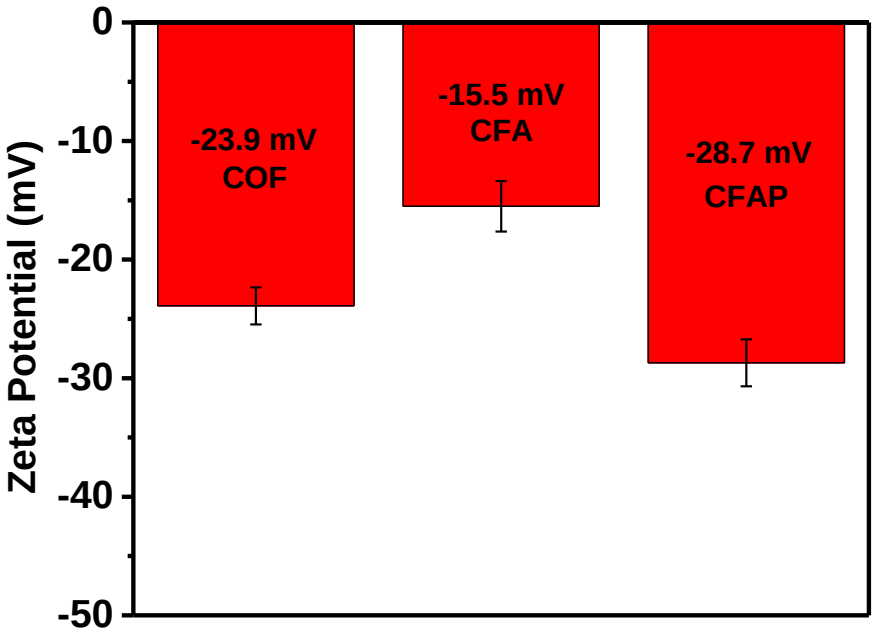

Figure S5. Zeta potentials of COF, CFA and CFAP, respectively.

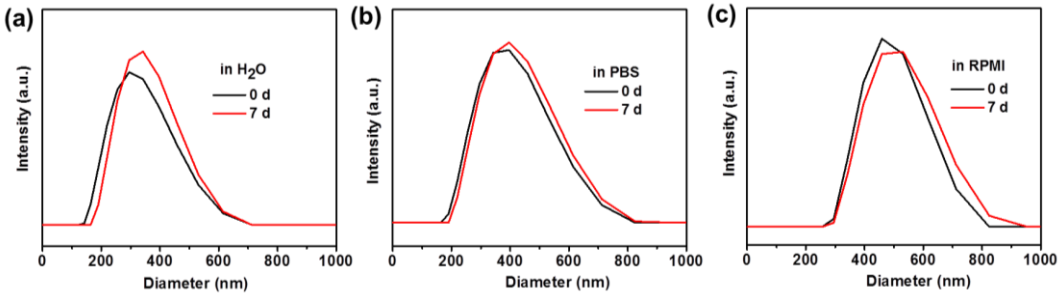

Figure S6. The DLS results of CFAP dispersed in (a) H_2O, (b) PBS and (c) RPMI, respectively.

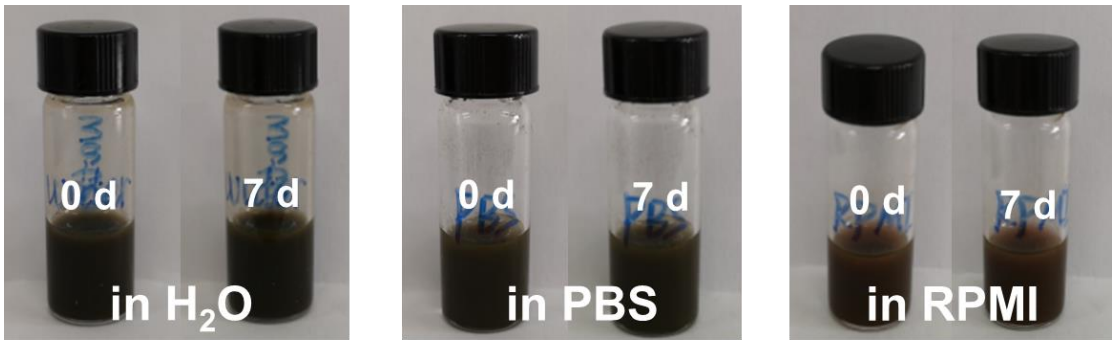

Figure S7. The photographs of CFAP dispersed in H_2O, PBS and RPMI, respectively.

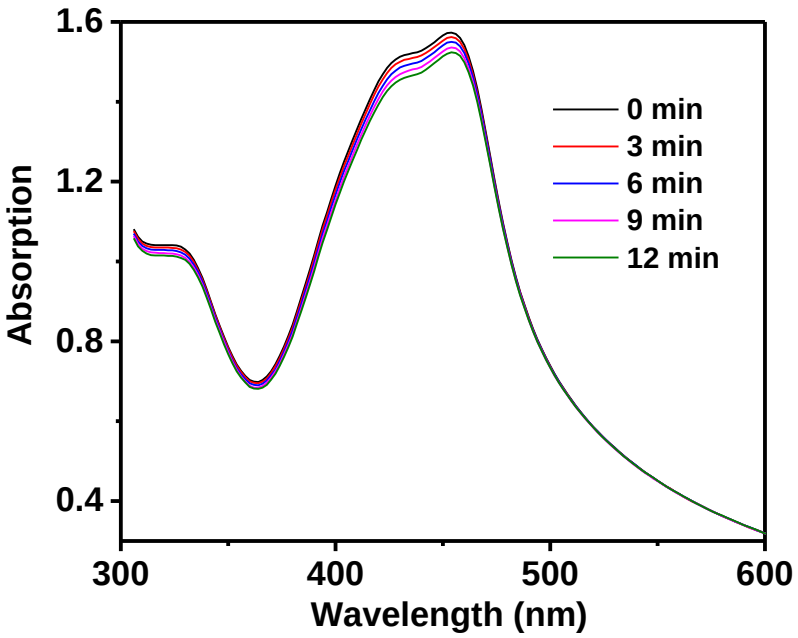

Figure S8. UV-Vis spectra of pure DPBF under laser irradiation (650 nm, 0.72 W cm^{-2}).

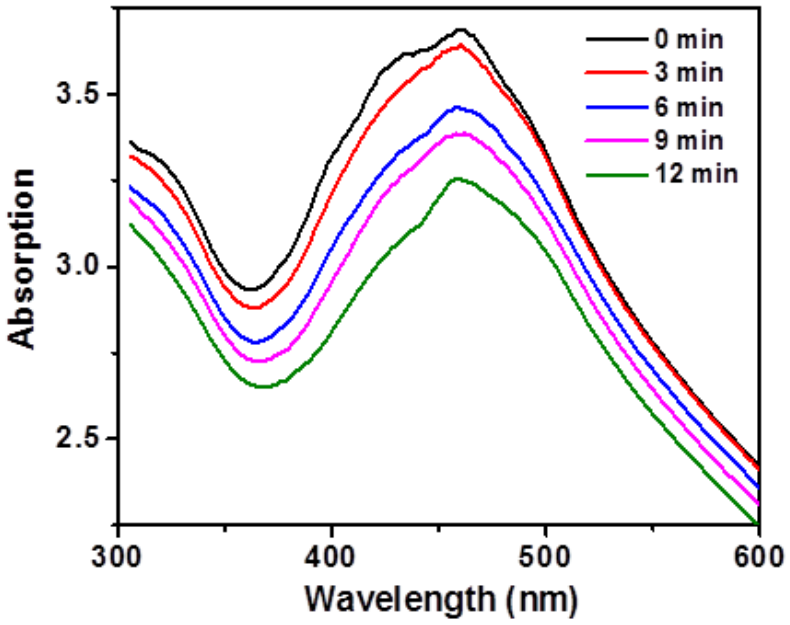

Figure S9. The UV-Vis spectra of DPBF in the presence of CFAP under laser irradiation (650 nm, 0.72 W cm^{-2}, 12 min).

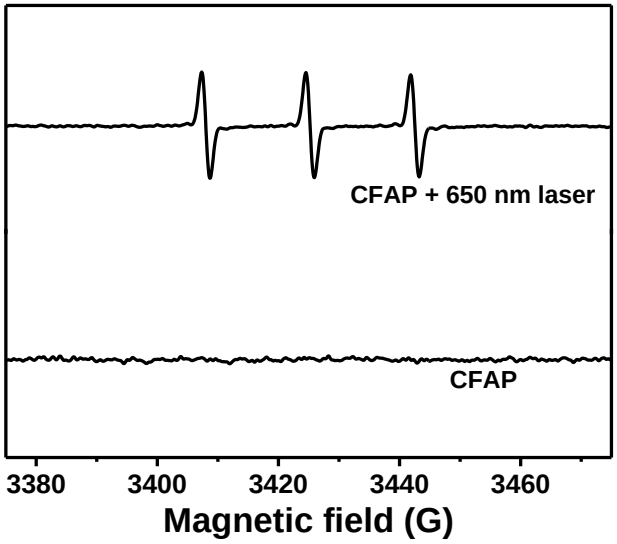

Figure S10. EPR spectra of CFAP and CFAP + 650 nm laser by using TMPO as a trapping agent.

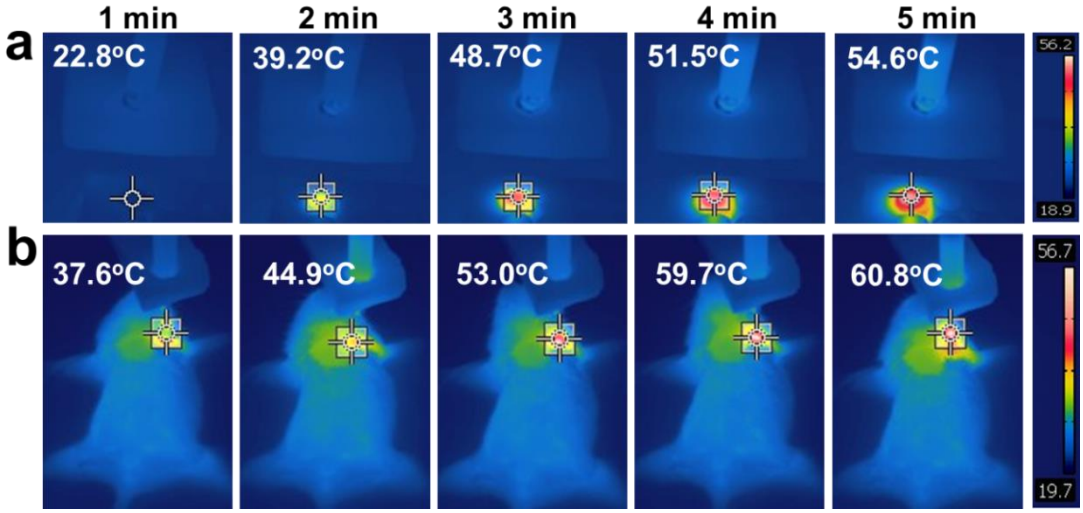

Figure S11. (a) Photographs of CFAP (400 μg mL^{-1}, in water) upon laser irradiation for different times. (b) The whole body photothermal images of mice after intratumoral injection of CFAP (0.1 mL, 400 μg mL^{-1}). Laser irradiation conditions: 808 nm and 1.56 W cm^{-2}.

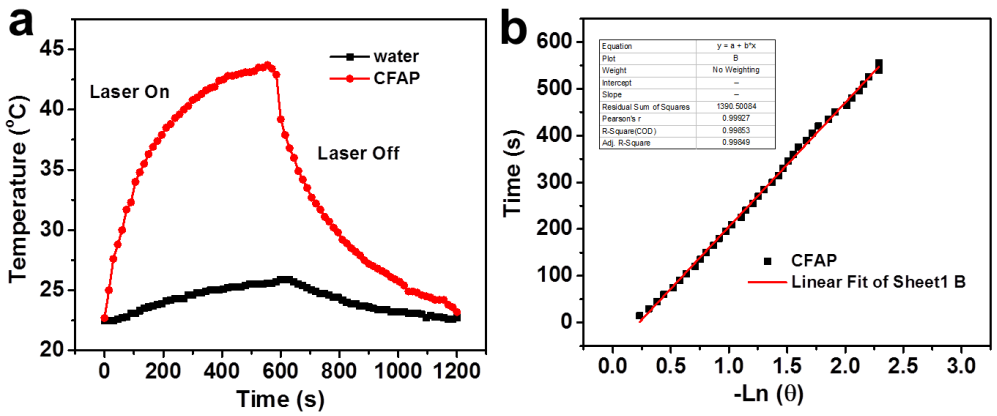

Figure S12. (a) Photothermal effect of CFAP aqueous solution (100 μg mL^{-1}) irradiated with an 808 nm CW laser (1.56 W cm^{-2}). (b) Linear fit of time/-ln(θ) obtained during the cooling process.

Table S1. Photothermal conversion efficiency for CFAP. Absorbance at irradiation wavelength ($A_{808\ nm}$), mass of solution (m sol), increasing temperature after CW laser irradiation (ΔT), time system constant (τ_s), thermal conductance (hS) and photothermal conversion efficiency (Efficiency).

Abs 808nm	m sol (g)	△T (K)	T_s (s)	hS (WK^{-1})	Efficiency (%)
1.496	1	18.8	265.124	0.0158	30.76

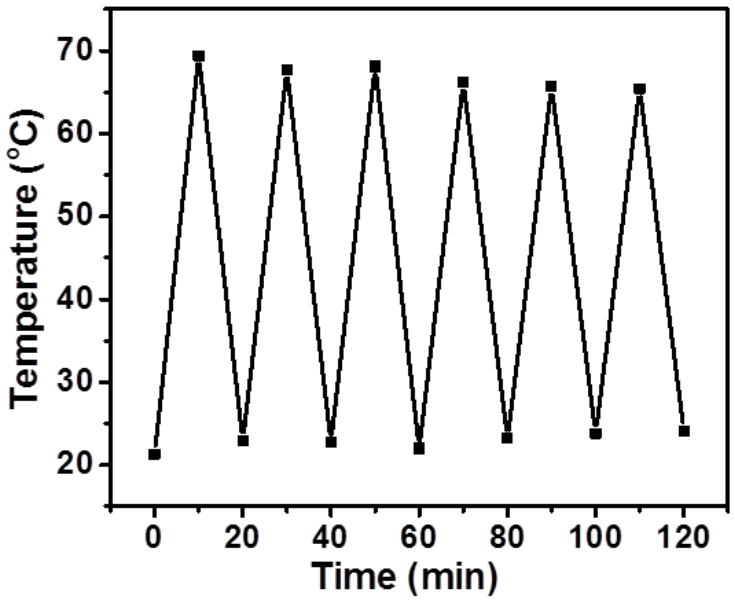

Figure S13. Photostability test of CFAP in 0.4 mL DI water.

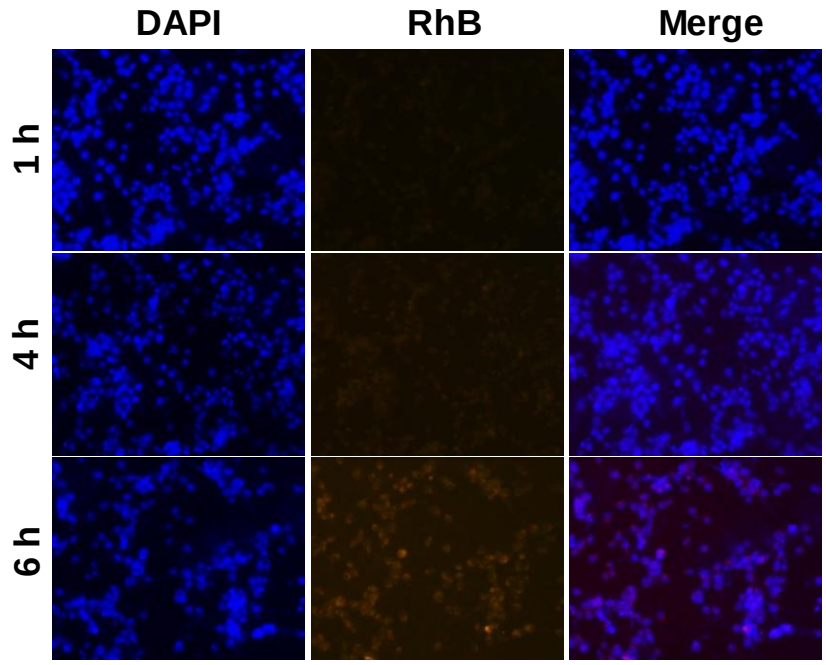

Figure S14. Fluorescence images of CT26 cells incubated with rhodamine B for 1, 4 and 6 h, respectively.

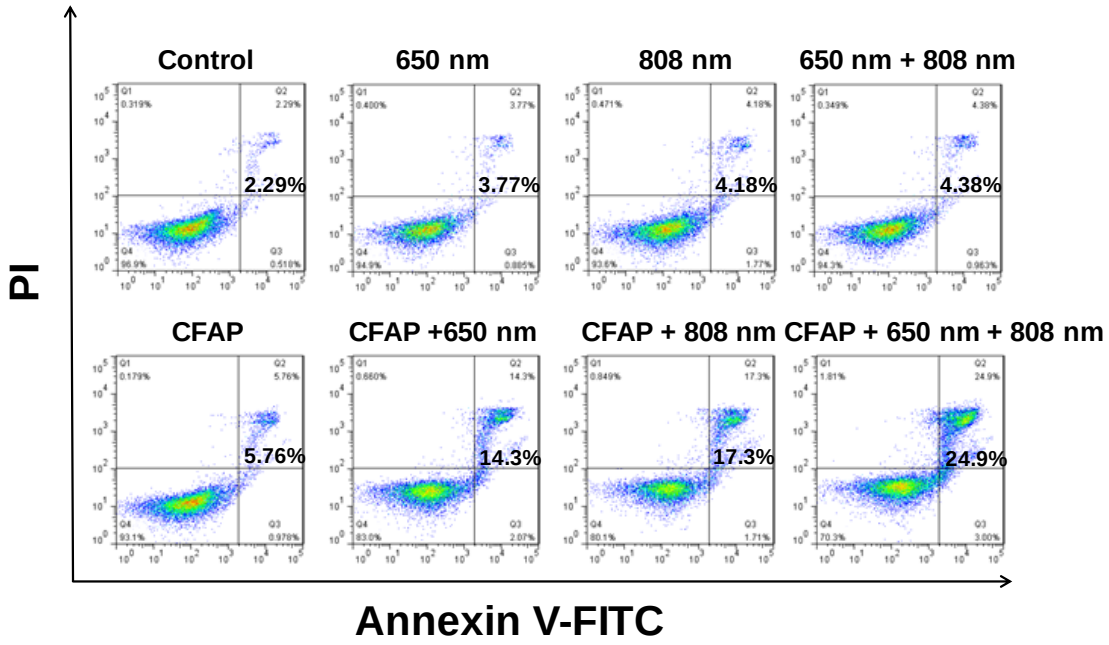

Figure S15. Flow cytometric analysis of CT26 cells treated with different methods.

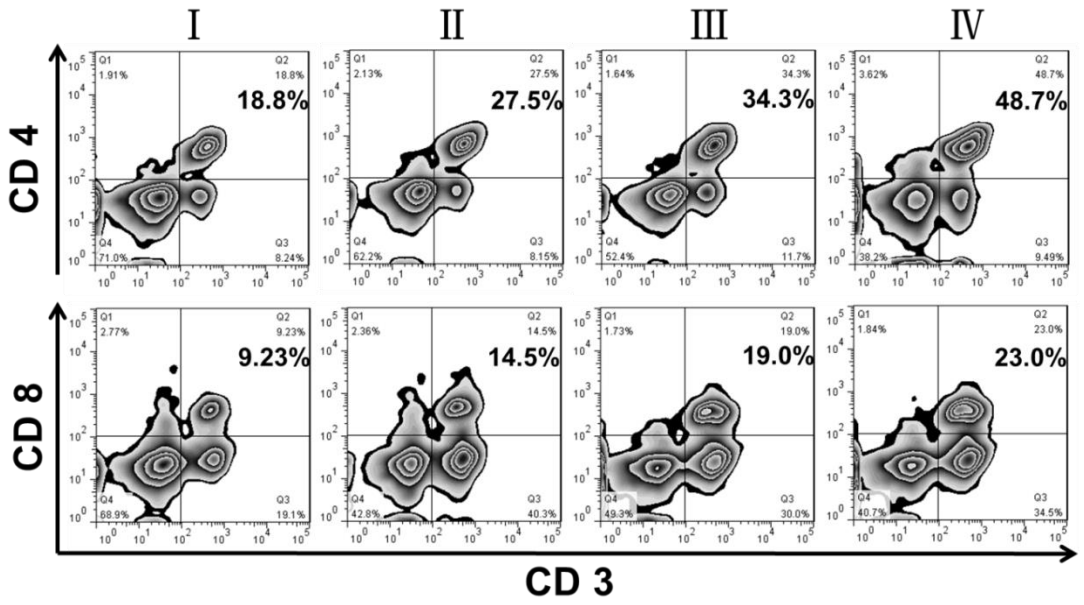

Figure S16. The flow cytometric analyses of the populations of CD4+ (CD3+CD4+ as the marker) and CD8+ (CD3+CD8+ as the marker) T cells in spleens of mice after various treatment. (Ⅰ, PBS; Ⅱ, PBS + anti-PD-L1; Ⅲ, CFAP + 650 nm + 808 nm; Ⅳ, CFAP + 650 nm + 808 nm + anti-PD L1).

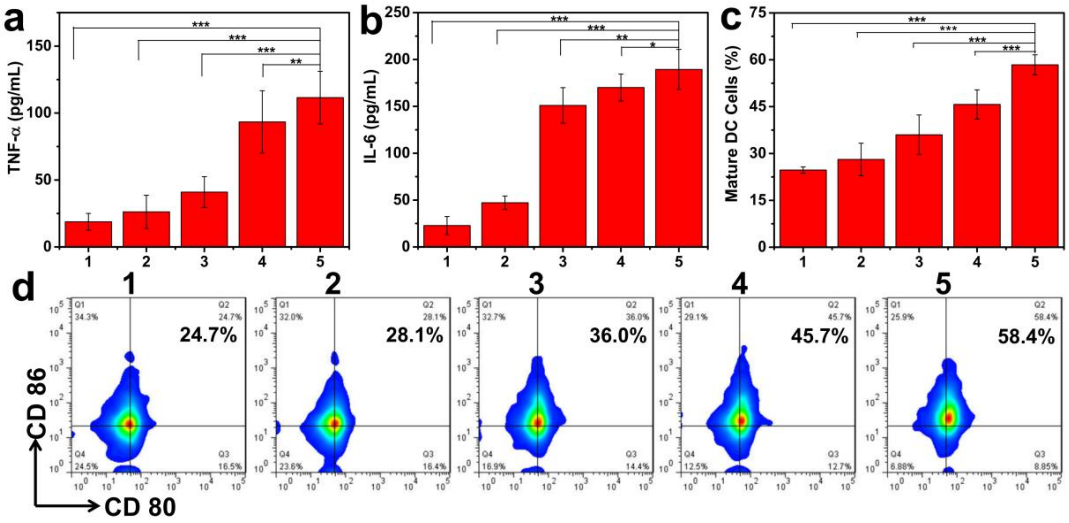

Figure S17. Cytokine levels of (a) TNF-α and (b) IL-6 in the supernatant of spleens for different groups. (c) and (d) DC maturation of lymph nodes from bilateral CT26 tumor bearing mice (n=5). (1: anti-PD-L1; 2: CFAP + anti-PD-L1; 3: CFAP + 650 nm + anti-PD-L1; 4: CFAP + 808 nm + anti-PD-L1; 5: CFAP + 650 nm + 808 nm + anti-PD-L1). The data were expressed as mean ± SD (n = 3), *p < 0.5; **p < 0.01; ***p < 0.001.

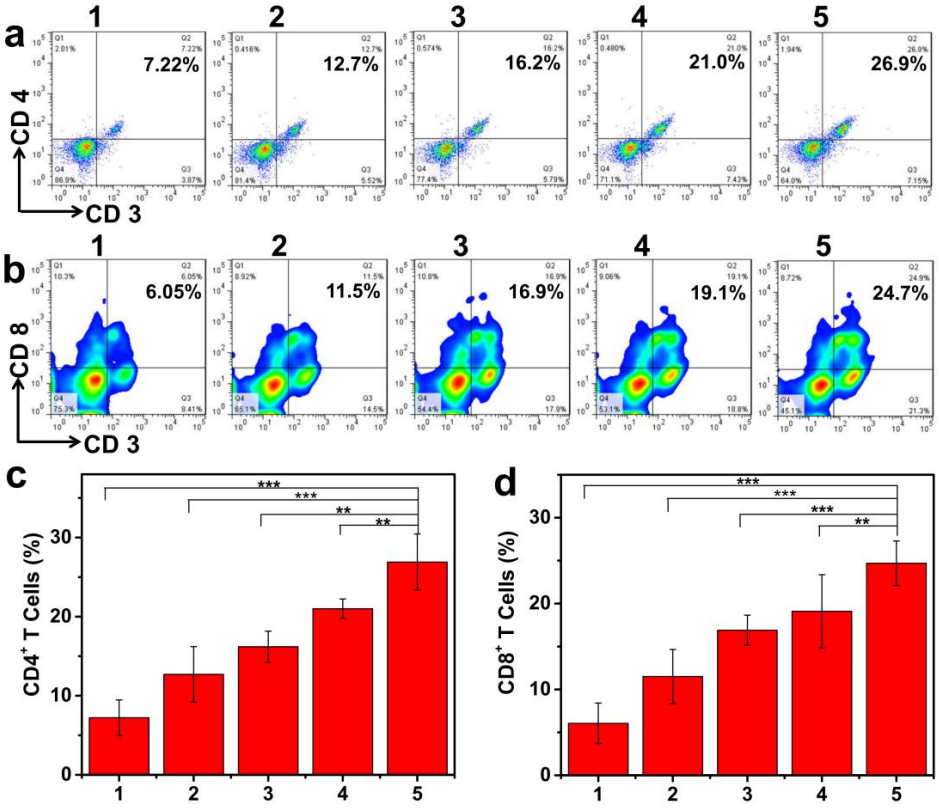

Figure S18. The flow cytometric analysis of (a) CD4+ (CD3+CD4+ as the marker) and (b) CD8+ (CD3+CD8+ as the marker) T cells in second tumors of mice after various treatments (n=5). The populations of (c) CD4+ and (d) CD8+ after different treatments. (1: anti-PD-L1; 2: CFAP + anti-PD-L1; 3: CFAP + 650 nm + anti-PD-L1; 4: CFAP + 808 nm + anti-PD-L1; 5: CFAP + 650 nm + 808 nm + anti-PD-L1). The data were expressed as mean ± SD (n = 3), *p < 0.5; **p < 0.01; ***p < 0.001.

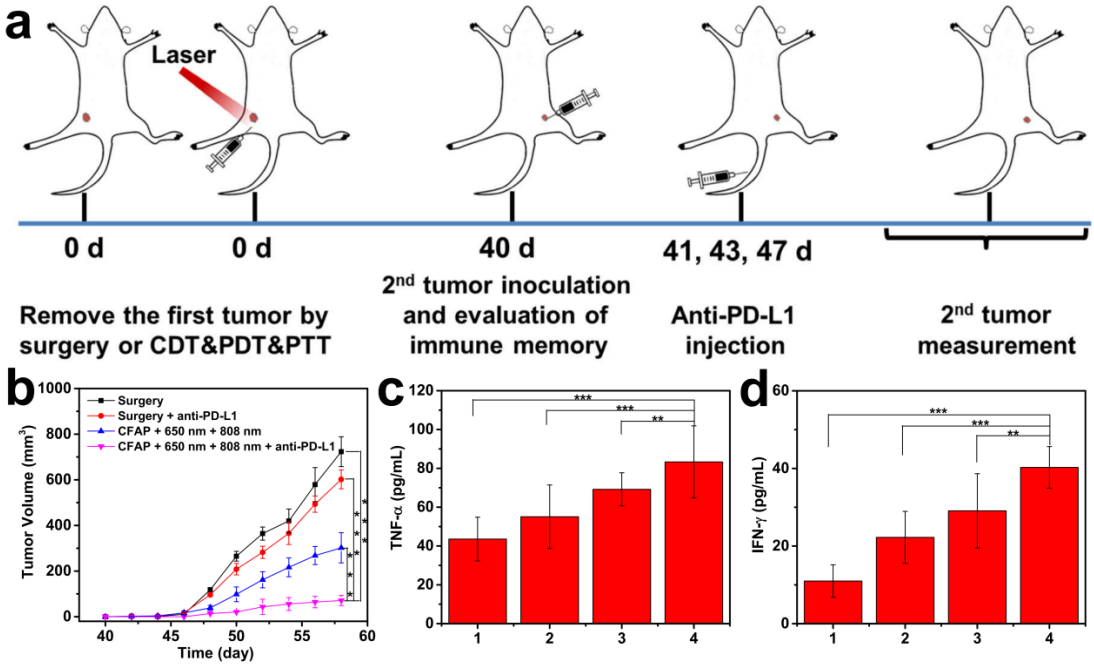

Figure S19. (a) Scheme of long-term immune memory effect in BALB/c mice. (b) Tumor growth curves of different groups. Cytokine levels of (c) TNF-α and (d) IFN-γ in the supernatant of spleens collected from mice treated with different methods on day 45 (n=3). (1: surgery; 2: surgery + anti-PD-L1; 3: CFAP + 650 nm + 808 nm; 4: CFAP + 650 nm + 808 nm + anti-PD-L1). The data were expressed as mean ± SD (n = 3), *p < 0.5; **p < 0.01; ***p < 0.001.

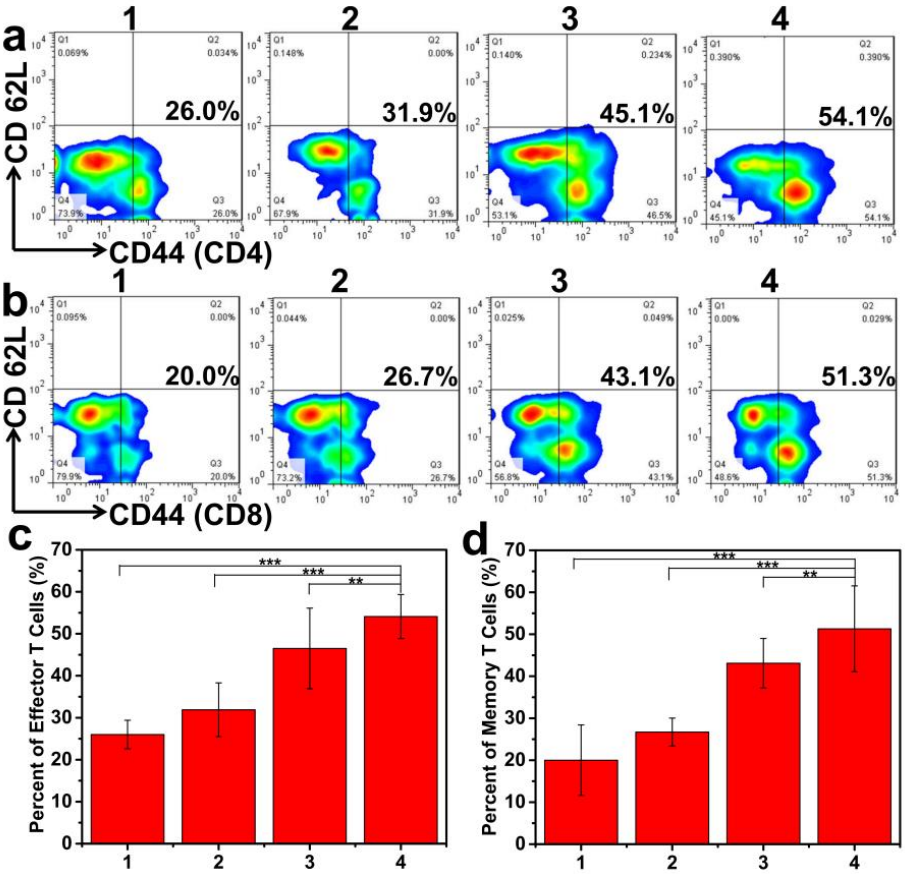

Figure S20. (a) Flow cytometry plots of effector (CD44+CD62L- as the marker, gated on CD4+) and (b) memory (CD44+CD62L- as the marker, gated on $CD8^+$) T cells in the spleen examined on day 40 (n=3). The populations of (c) effector T cells and (d) memory T cells after different treatments. (1: surgery; 2: surgery + anti-PD-L1; 3: CFAP + 650 nm + 808 nm; 4: CFAP + 650 nm + 808 nm + anti-PD-L1). The data were expressed as mean ± SD (n = 3), *p < 0.5; **p < 0.01; ***p < 0.001.